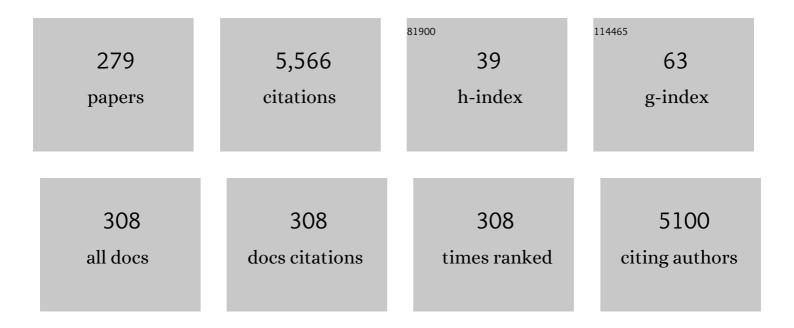
List of Publications by Year in descending order

Source: https://exaly.com/author-pdf/2019618/publications.pdf Version: 2024-02-01



#	Article	IF	CITATIONS
1	Quantitative Analysis of Pleural Line and B-Lines in Lung Ultrasound Images for Severity Assessment of COVID-19 Pneumonia. IEEE Transactions on Ultrasonics, Ferroelectrics, and Frequency Control, 2022, 69, 73-83.	3.0	11
2	Acceleration of reconstruction for compressed sensing based synthetic transmit aperture imaging by using in-phase/quadrature data. Ultrasonics, 2022, 118, 106576.	3.9	6
3	Deep weakly-supervised breast tumor segmentation in ultrasound images with explicit anatomical constraints. Medical Image Analysis, 2022, 76, 102315.	11.6	20
4	Improved Ultrasound Imaging Performance with Complex Cumulant Analysis. IEEE Transactions on Biomedical Engineering, 2022, PP, 1-1.	4.2	1
5	Hadamard-Encoded Synthetic Transmit Aperture Imaging for Improved Lateral Motion Estimation in Ultrasound Elastography. IEEE Transactions on Ultrasonics, Ferroelectrics, and Frequency Control, 2022, 69, 1204-1218.	3.0	3
6	Improved Ultrafast Power Doppler Imaging by Using Spatiotemporal Non-Local Means Filtering. IEEE Transactions on Ultrasonics, Ferroelectrics, and Frequency Control, 2022, 69, 1610-1624.	3.0	17
7	In vivo assessment of hypertensive nephrosclerosis using ultrasound localization microscopy. Medical Physics, 2022, 49, 2295-2308.	3.0	16
8	Partial Hadamard encoded synthetic transmit aperture for high frame rate imaging with minimal l <sub>2</sub> -norm least squares method. Physics in Medicine and Biology, 2022, 67, 105002.	3.0	4
9	Unsupervised Convolutional Neural Network for Motion Estimation in Ultrasound Elastography. IEEE Transactions on Ultrasonics, Ferroelectrics, and Frequency Control, 2022, 69, 2236-2247.	3.0	10
10	SAturationâ€recovery and Variableâ€flipâ€Angle (SAVA) based threeâ€dimensional freeâ€breathing cardiovascular magnetic resonance T <sub>1</sub> mapping at 3T. NMR in Biomedicine, 2022, , e4755.	2.8	1
11	A novel rat model of cerebral small vessel disease and evaluation by super-resolution ultrasound imaging. Journal of Neuroscience Methods, 2022, 379, 109673.	2.5	2
12	Multi-segmented feature coupling for jointly reconstructing initial pressure and speed of sound in photoacoustic computed tomography. Journal of Biomedical Optics, 2022, 27, .	2.6	1
13	Influence of key parameters on motion artifacts in lateral strain estimation with spatial angular compounding. Ultrasonics, 2022, 125, 106799.	3.9	0
14	Reconstructing Undersampled Photoacoustic Microscopy Images Using Deep Learning. IEEE Transactions on Medical Imaging, 2021, 40, 562-570.	8.9	71
15	ApodNet: Learning for High Frame Rate Synthetic Transmit Aperture Ultrasound Imaging. IEEE Transactions on Medical Imaging, 2021, 40, 3190-3204.	8.9	20
16	A Novel Normalized Cross-Correlation Speckle-Tracking Ultrasound Algorithm for the Evaluation of Diaphragm Deformation. Frontiers in Medicine, 2021, 8, 612933.	2.6	3
17	Adaptive photoacoustic computed tomography. Photoacoustics, 2021, 21, 100223.	7.8	18
18	Photoacoustic imaging of in vivo hemodynamic responses to sodium nitroprusside. Journal of Biophotonics, 2021, 14, e202000478.	2.3	5

#	Article	IF	CITATIONS
19	Ultrasound image reconstruction from plane wave radio-frequency data by self-supervised deep neural network. Medical Image Analysis, 2021, 70, 102018.	11.6	46
20	Improving the Subtype Classification of Non-small Cell Lung Cancer by Elastic Deformation Based Machine Learning. Journal of Digital Imaging, 2021, 34, 605-617.	2.9	8
21	Depth-recognizable time-domain fluorescence molecular tomography in reflective geometry. Biomedical Optics Express, 2021, 12, 3806.	2.9	4
22	Deep image prior for undersampling high-speed photoacoustic microscopy. Photoacoustics, 2021, 22, 100266.	7.8	33
23	Perivascular Space Detection by Using Contrast-enhanced Ultrafast Power Doppler Imaging: A Feasibility Study. , 2021, , .		0
24	A General Framework for Inverse Problem Solving using Self-Supervised Deep Learning: Validations in Ultrasound and Photoacoustic Image Reconstruction. , 2021, , .		5
25	Ultrasound Image Reconstruction by Self-Supervised Deep Neural Network A Study on Coherent Compounding Strategy. , 2021, , .		1
26	Weakly-supervised deep learning for breast tumor segmentation in ultrasound images. , 2021, , .		0
27	A Self-supervised Deep Learning Approach for High Frame Rate Plane Wave Beamforming with Two-way Dynamic Focusing. , 2021, , .		0
28	Localization of High-concentration Microbubbles for Ultrasound Localization Microscopy by Self-Supervised Deep Learning. , 2021, , .		6
29	In Vivo Assessment of Diabetic Kidney Disease using Ultrasound Localization Microscopy. , 2021, , .		2
30	Partial Hadamard Encoded Synthetic Transmit Aperture for High Frame Rate Imaging with Minimal l2-Norm Least Square Method. , 2021, , .		1
31	Improved Background Noise Suppression in Ultrasound Localization Microscopy using Spatial Coherence Beamforming. , 2021, , .		5
32	Semi-supervised deep learning for breast anatomy decomposition in ultrasound images. , 2021, , .		1
33	Pleural line and B-lines based image analysis for severity evaluation of COVID-19 pneumonia. , 2021, , .		2
34	Hadamard-encoded synthetic transmit aperture imaging for improvement of strain estimation. , 2021, , .		0
35	Recovery of Full Synthetic Transmit Aperture Dataset with Well-preserved Phase Information by Self-supervised Deep Learning. , 2021, , .		1
36	Contrast-free Ultrasound Microvascular Imaging for Intraoperative Detection of Human Spinal Cord Tumor: An In vivo Feasibility Study. , 2021, , .		8

#	Article	IF	CITATIONS
37	Phase Constraint Improves Ultrasound Image Quality Reconstructed using Deep Neural Network. , 2021, , .		3
38	Deep Unfolded Robust PCA With Application to Clutter Suppression in Ultrasound. IEEE Transactions on Medical Imaging, 2020, 39, 1051-1063.	8.9	117
39	Radiomics With Attribute Bagging for Breast Tumor Classification Using Multimodal Ultrasound Images. Journal of Ultrasound in Medicine, 2020, 39, 361-371.	1.7	29
40	Accurate detection of atrial fibrillation from 12-lead ECG using deep neural network. Computers in Biology and Medicine, 2020, 116, 103378.	7.0	67
41	Self-Supervised Learning of a Deep Neural Network for Ultrafast Ultrasound Imaging as an Inverse Problem. , 2020, , .		6
42	Highly-efficient quantitative fluorescence resonance energy transfer measurements based on deep learning. Journal of Innovative Optical Health Sciences, 2020, 13, 2050021.	1.0	2
43	Fast Randomized Singular Value Decomposition-Based Clutter Filtering for Shear Wave Imaging. IEEE Transactions on Ultrasonics, Ferroelectrics, and Frequency Control, 2020, 67, 2363-2377.	3.0	5
44	Deep Learning for Ultrasound Localization Microscopy. IEEE Transactions on Medical Imaging, 2020, 39, 3064-3078.	8.9	72
45	qULM-DL: Quantitative Ultrasound Localization Microscopy via Deep Learning. , 2020, , .		2
46	Tikhonov-regularization-based projecting sparsity pursuit method for fluorescence molecular tomography reconstruction. Chinese Optics Letters, 2020, 18, 011701.	2.9	6
47	A Deep Learning Method for Reduction of Microbubble Accumulation Time in Ultrasound Localization Microscopy. , 2020, , .		2
48	A 3D Motion Compensation Method for High Frame Rate Volumetric Ultrasound Imaging based on Velocity Vector Estimation: A Simulation Study. , 2020, , .		3
49	Intraoperative Ultrasound Localization Microscopy of Human Spinal Cord: An In Vivo Feasibility Study. , 2020, , .		1
50	Feature coupling photoacoustic computed tomography for joint reconstruction of initial pressure and sound speed in vivo. Biomedical Optics Express, 2019, 10, 3447.	2.9	23
51	Learning the implicit strain reconstruction in ultrasound elastography using privileged information. Medical Image Analysis, 2019, 58, 101534.	11.6	56
52	Evaluating HIFUâ€mediated local drug release using thermal strain imaging: Phantom and preliminary <i>inâ€vivo</i> studies. Medical Physics, 2019, 46, 3864-3876.	3.0	11
53	Spatial Angular Compounding With Affine-Model-Based Optical Flow for Improvement of Motion Estimation. IEEE Transactions on Ultrasonics, Ferroelectrics, and Frequency Control, 2019, 66, 701-716.	3.0	9
54	Super-Resolution Ultrasound Imaging by Sparse Bayesian Learning Method. IEEE Access, 2019, 7, 47197-47205.	4.2	5

#	Article	IF	CITATIONS
55	Coded Excitation for Crosstalk Suppression in Multi-line Transmit Beamforming: Simulation Study and Experimental Validation. Applied Sciences (Switzerland), 2019, 9, 486.	2.5	11
56	Pulse Wave Imaging for Assessing Arterial Stiffness Change in A Mouse Model of Thoracic Aortic Dissection in Marfan Syndrome. , 2019, , .		1
57	A Comparative Study of Direct and Iterative Inversion Approaches to Determine the Spatial Shear Modulus Distribution of Elastic Solids. International Journal of Applied Mechanics, 2019, 11, 1950097.	2.2	12
58	Non-rigid Motion Correction for Ultrasound Localization Microscopy of the Liver in vivo. , 2019, , .		15
59	An in vivo Comparison of Principal and Polar Strains in Carotid Atherosclerotic Plaques. , 2019, , .		Ο
60	Multi-plane-transmit (MPT) Volumetric Imaging based on A Matrix Array: Experimental Validation. , 2019, , .		0
61	Interoperator Reproducibility of Carotid Elastography for Identification of Vulnerable Atherosclerotic Plaques. IEEE Transactions on Ultrasonics, Ferroelectrics, and Frequency Control, 2019, 66, 505-516.	3.0	15
62	A threeâ€dimensional freeâ€breathing sequence for simultaneous myocardial T <sub>1</sub> and T <sub>2</sub> mapping. Magnetic Resonance in Medicine, 2019, 81, 1031-1043.	3.0	25
63	Compressed sensing reconstruction of synthetic transmit aperture dataset for volumetric diverging wave imaging. Physics in Medicine and Biology, 2019, 64, 025013.	3.0	13
64	Streak artifact suppression in photoacoustic computed tomography using adaptive back projection. Biomedical Optics Express, 2019, 10, 4803.	2.9	13
65	Thermal memory based photoacoustic imaging of temperature. Optica, 2019, 6, 198.	9.3	44
66	Photoacoustic computed tomography for joint reconstruction of initial pressure and sound speed in vivo using a feature coupling method. , 2019, , .		1
67	Machine-learning enhanced photoacoustic computed tomography in a limited view configuration. , 2019, , .		6
68	2-D Myocardial Deformation Imaging Based on RF-Based Nonrigid Image Registration. IEEE Transactions on Ultrasonics, Ferroelectrics, and Frequency Control, 2018, 65, 1037-1047.	3.0	10
69	Generalized Adaptive Gaussian Markov Random Field for X-Ray Luminescence Computed Tomography. IEEE Transactions on Biomedical Engineering, 2018, 65, 2130-2133.	4.2	19
70	Quantitative evaluation of graded hindlimb ischemia based on pharmacokinetic modelling and hemodynamic analysis of indocyanine green. Physiological Measurement, 2018, 39, 015009.	2.1	0
71	Compressed Sensing Based Synthetic Transmit Aperture for Phased Array Using Hadamard Encoded Diverging Wave Transmissions. IEEE Transactions on Ultrasonics, Ferroelectrics, and Frequency Control, 2018, 65, 1141-1152.	3.0	17
72	Robust Segmentation of Intima–Media Borders With Different Morphologies and Dynamics During the Cardiac Cycle. IEEE Journal of Biomedical and Health Informatics, 2018, 22, 1571-1582.	6.3	55

#	Article	IF	CITATIONS
73	Compressed Sensing Based Synthetic Transmit Aperture Imaging: Validation in a Convex Array Configuration. IEEE Transactions on Ultrasonics, Ferroelectrics, and Frequency Control, 2018, 65, 300-315.	3.0	22
74	Correcting the limited view in opticalâ€resolution photoacoustic microscopy. Journal of Biophotonics, 2018, 11, e201700196.	2.3	15
75	Cardiac Deformation Imaging Based on Coherent Compounding of Diverging Waves with Coded Excitation. , 2018, , .		1
76	Assessment of Diabetic Kidney Disease Using Ultrasound Localization Microscopy: An in Vivo Feasibility Study in Rats. , 2018, , .		10
77	Influence of Factors on Motion Artifacts in Strain Estimation with Spatial Angular Compounding. , 2018, , .		0
78	S-Sequence Encoded Multiplane Wave Imaging: Phantom and In-Vivo Validation. , 2018, , .		1
79	2D Motion Estimation Based on Diverging Wave Coherent Compounding and Transverse Oscillations. , 2018, , .		1
80	High-Quality Reconstruction of Plane-Wave Imaging Using Generative Adversarial Network. , 2018, , .		21
81	A Deep Learning Trial on Transient Elastography for Assessment of Liver Fibrosis. , 2018, , .		5
82	Electromagnetic tracking-based freehand 3D quasi-static elastography with 1D linear array: a phantom study. Physics in Medicine and Biology, 2018, 63, 245006.	3.0	4
83	Performance Optimization of Compressed Sensing Based Synthetic Transmit Aperture Using Hadamard Matrix Encoding. , 2018, , .		1
84	Three-dimensional free breathing whole heart cardiovascular magnetic resonance T1 mapping at 3ÂT. Journal of Cardiovascular Magnetic Resonance, 2018, 20, 64.	3.3	22
85	Direct Reconstruction of Ultrasound Elastography Using an End-to-End Deep Neural Network. Lecture Notes in Computer Science, 2018, , 374-382.	1.3	33
86	Diverging wave compounding with spatio-temporal encoding using orthogonal Golay pairs for high frame rate imaging. Ultrasonics, 2018, 89, 155-165.	3.9	10
87	Doppler-Based Motion Compensation Strategies for 3-D Diverging Wave Compounding and Multiplane-Transmit Beamforming: A Simulation Study. IEEE Transactions on Ultrasonics, Ferroelectrics, and Frequency Control, 2018, 65, 1631-1642.	3.0	12
88	End-to-end deep neural network for optical inversion in quantitative photoacoustic imaging. Optics Letters, 2018, 43, 2752.	3.3	95
89	Deep-tissue temperature mapping by multi-illumination photoacoustic tomography aided by a diffusion optical model: a numerical study. Journal of Biomedical Optics, 2018, 23, 1.	2.6	8
90	Reconstruction of high-resolution early-photon tomography based on the first derivative of temporal point spread function. Journal of Biomedical Optics, 2018, 23, 1.	2.6	7

#	Article	IF	CITATIONS
91	A net-shaped multicellular formation facilitates the maturation of hPSC-derived cardiomyocytes through mechanical and electrophysiological stimuli. Aging, 2018, 10, 532-548.	3.1	6
92	Enhancing in vivo renal ischemia assessment by high-dynamic-range fluorescence molecular imaging. Journal of Biomedical Optics, 2018, 23, 1.	2.6	0
93	Deep learning for super-resolution localization microscopy. , 2018, , .		0
94	Multiparametric evaluation of hindlimb ischemia using time-series indocyanine green fluorescence imaging. Journal of Biophotonics, 2017, 10, 456-464.	2.3	8
95	Non-Invasive Identification of Vulnerable Atherosclerotic Plaques Using Texture Analysis in Ultrasound Carotid Elastography: An InÂVivo Feasibility Study Validated by Magnetic Resonance Imaging. Ultrasound in Medicine and Biology, 2017, 43, 817-830.	1.5	25
96	A Noninvasive Sonographic Study of Multisite Atherosclerosis in an Elderly Chinese Population. Journal of Ultrasound in Medicine, 2017, 36, 639-647.	1.7	3
97	Feasibility of Multiplane-Transmit Beamforming for Real-Time Volumetric Cardiac Imaging: A Simulation Study. IEEE Transactions on Ultrasonics, Ferroelectrics, and Frequency Control, 2017, 64, 648-659.	3.0	15
98	Guided waves in pre-stressed hyperelastic plates and tubes: Application to the ultrasound elastography of thin-walled soft materials. Journal of the Mechanics and Physics of Solids, 2017, 102, 67-79.	4.8	40
99	Coded excitation for diverging wave cardiac imaging: a feasibility study. Physics in Medicine and Biology, 2017, 62, 1565-1584.	3.0	18
100	Novel Method for Vessel Cross-Sectional Shear Wave Imaging. Ultrasound in Medicine and Biology, 2017, 43, 1520-1532.	1.5	15
101	Enhanced imaging resolution in dynamic fluorescence molecular tomography by multispectral excitation method (Conference Presentation). , 2017, , .		0
102	An Inverse Method to Determine Arterial Stiffness with Guided Axial Waves. Ultrasound in Medicine and Biology, 2017, 43, 505-516.	1.5	23
103	A Systematic Investigation of Lateral Estimation Using Various Interpolation Approaches in Conventional Ultrasound Imaging. IEEE Transactions on Ultrasonics, Ferroelectrics, and Frequency Control, 2017, 64, 1149-1160.	3.0	25
104	Spread spectrum time-resolved diffuse optical measurement system for enhanced sensitivity in detecting human brain activity. Journal of Biomedical Optics, 2017, 22, 045005.	2.6	10
105	Excitation-resolved multispectral method for imaging pharmacokinetic parameters in dynamic fluorescent molecular tomography. Journal of Biomedical Optics, 2017, 22, 046003.	2.6	3
106	Effects of temperature on multiparametric evaluation of hindlimb ischemia with dynamic fluorescence imaging. Journal of Biophotonics, 2017, 10, 811-820.	2.3	5
107	A Compressed Sensing Strategy for Synthetic Transmit Aperture Ultrasound Imaging. IEEE Transactions on Medical Imaging, 2017, 36, 878-891.	8.9	53
108	An ultrasound elastography method to determine the local stiffness of arteries with guided circumferential waves. Journal of Biomechanics, 2017, 51, 97-104.	2.1	23

#	Article	IF	CITATIONS
109	Tumor-homing, pH- and ultrasound-responsive polypeptide-doxorubicin nanoconjugates overcome doxorubicin resistance in cancer therapy. Journal of Controlled Release, 2017, 264, 66-75.	9.9	58
110	Performance comparison of optical flow and block matching methods in shearing and rotating models. Proceedings of SPIE, 2017, , .	0.8	0
111	Performance optimization of lateral displacement estimation with spatial angular compounding. Ultrasonics, 2017, 73, 9-21.	3.9	18
112	Cone Beam X-ray Luminescence Computed Tomography Based on Bayesian Method. IEEE Transactions on Medical Imaging, 2017, 36, 225-235.	8.9	43
113	Motion compensation and sequence optimization for 3D diverging wave compounding: A simulation study. Proceedings of Meetings on Acoustics, 2017, , .	0.3	0
114	Notice of Removal: Performance comparison of optical flow and block matching methods for strain estimation in spatial angular compounding with plane wave. , 2017, , .		0
115	Notice of Removal: Suppression of reflected waves with high-resolution Radon transform for accurate measurement of regional pulse wave velocity. , 2017, , .		0
116	Notice of Removal: Orthogonal Golay pairs-coded diverging wave compounding for high-quality and high-frame-rate ultrasound imaging. , 2017, , .		0
117	An optical flow method for elastography at large strains using three image frames. , 2017, , .		0
118	Notice of Removal: Guided wave elastography of press-stressed thin-walled soft tissues. , 2017, , .		0
119	Self-prior strategy for organ reconstruction in fluorescence molecular tomography. Biomedical Optics Express, 2017, 8, 4671.	2.9	9
120	Notice of Removal: An MRI-compatible mock model for intra-cardiac flow imaging. , 2017, , .		0
121	Notice of Removal: Motion correction for multi-plane-transmit beamforming: A simulation study. , 2017, , .		0
122	Compressed sensing based synthetic transmit aperture for phased array imaging. , 2017, , .		0
123	Compressed sensing based synthetic transmit aperture for phased array imaging. , 2017, , .		1
124	An optical flow method for elastography at large compression using three image frames. , 2017, , .		0
125	Comparison of different motion estimation methods for vessel cross-sectional shear wave imaging. , 2017, , .		0
126	Notice of Removal: Guided wave elastography of pressurized artery in both longitudinal and		0

transverse sections: Validation in phantom experiments. , 2017, , .

#	Article	IF	CITATIONS
127	Notice of Removal: Archimedean spiral based compounding for high quality and high frame rate convex array imaging. , 2017, , .		0
128	Notice of Removal: Feasibility of thermal strain imaging in noninvasive monitoring of HIFU-mediated local drug delivery. , 2017, , .		1
129	Comparison of different motion estimation methods for vessel cross-sectional shear wave imaging. , 2017, , .		Ο
130	Notice of Removal: Comparison of motion corrected multi-plane-transmit beamforming and 3D diverging wave compounding: A simulation study. , 2017, , .		0
131	Facilitating in vivo tumor localization by principal component analysis based on dynamic fluorescence molecular imaging. Journal of Biomedical Optics, 2017, 22, 1.	2.6	5
132	Evaluating the Significance of Viscoelasticity in Diagnosing Early-Stage Liver Fibrosis with Transient Elastography. PLoS ONE, 2017, 12, e0170073.	2.5	16
133	Nonlinear greedy sparsity-constrained algorithm for direct reconstruction of fluorescence molecular lifetime tomography. Biomedical Optics Express, 2016, 7, 1210.	2.9	7
134	Automatic selection of regularization parameters for dynamic fluorescence molecular tomography: a comparison of L-curve and U-curve methods. Biomedical Optics Express, 2016, 7, 5021.	2.9	17
135	Identification of early atherosclerotic lesions in carotid arteries with quantitative characteristics measured by 3D MRI. Journal of Magnetic Resonance Imaging, 2016, 44, 1270-1276.	3.4	4
136	Spectral selective fluorescence molecular imaging with volume holographic imaging system. Journal of Innovative Optical Health Sciences, 2016, 09, 1650010.	1.0	4
137	Multispectral excitation based multiple fluorescent targets resolving in fluorescence molecular tomography. Proceedings of SPIE, 2016, , .	0.8	О
138	Self-guided reconstruction for time-domain fluorescence molecular lifetime tomography. Journal of Biomedical Optics, 2016, 21, 126012.	2.6	4
139	2D RF-based non-rigid image registration for cardiac motion estimation: Comparison against block matching. , 2016, , .		3
140	Reconstruction of in vivo fluorophore concentration variation with structural priors and smooth penalty. Applied Optics, 2016, 55, 2732.	2.1	5
141	Elastic Cherenkov effects in transversely isotropic soft materials-II: Ex vivo and in vivo experiments. Journal of the Mechanics and Physics of Solids, 2016, 94, 181-190.	4.8	13
142	Reduction of blurring in broadband volume holographic imaging using a deconvolution method. Biomedical Optics Express, 2016, 7, 3124.	2.9	3
143	Unmixing multiple adjacent fluorescent targets with multispectral excited fluorescence molecular tomography. Applied Optics, 2016, 55, 4843.	2.1	7
144	Tunable narrowband volume holographic imaging spectrometer for macroscopic fluorescence molecular tomography. Optical Engineering, 2016, 55, 123113.	1.0	1

#	Article	IF	CITATIONS
145	Noninvasive measurement of regional pulse wave velocity in human ascending aorta with ultrasound imaging. Journal of Hypertension, 2016, 34, 2026-2037.	0.5	13
146	Fast direct reconstruction strategy of dynamic fluorescence molecular tomography using graphics processing units. Journal of Biomedical Optics, 2016, 21, 066010.	2.6	4
147	In vivosimultaneous multispectral fluorescence imaging with spectral multiplexed volume holographic imaging system. Journal of Biomedical Optics, 2016, 21, 060502.	2.6	5
148	Shape-based reconstruction of dynamic fluorescent yield with a level set method. BioMedical Engineering OnLine, 2016, 15, 6.	2.7	3
149	Wide-Angle Tissue Doppler Imaging at High Frame Rate Using Multi-Line Transmit Beamforming: An Experimental Validation In Vivo. IEEE Transactions on Medical Imaging, 2016, 35, 521-528.	8.9	33
150	High frame rate and high line density ultrasound imaging for local pulse wave velocity estimation using motion matching: A feasibility study on vessel phantoms. Ultrasonics, 2016, 67, 41-54.	3.9	12
151	Iterative Correction Scheme Based on Discrete Cosine Transform and L1 Regularization for Fluorescence Molecular Tomography With Background Fluorescence. IEEE Transactions on Biomedical Engineering, 2016, 63, 1107-1115.	4.2	13
152	Comparison of Different Pulse Waveforms for Local Pulse Wave Velocity Measurement in Healthy and Hypertensive Common Carotid Arteries inÂVivo. Ultrasound in Medicine and Biology, 2016, 42, 1111-1123.	1.5	23
153	Ultrasound-Based Carotid Elastography for Detection ofÂVulnerable Atherosclerotic Plaques Validated by MagneticÂResonance Imaging. Ultrasound in Medicine and Biology, 2016, 42, 365-377.	1.5	61
154	Early-photon guided reconstruction method for time-domain fluorescence lifetime tomography. Chinese Optics Letters, 2016, 14, 071702.	2.9	6
155	Compact multispectral fluorescence imaging system with spectral multiplexed volume holographic grating. Proceedings of SPIE, 2016, , .	0.8	0
156	Performance comparison of rigid and affine models for motion estimation using ultrasound RF signals: Simulations and phantom experiments. , 2015, , .		0
157	Fast reconstruction of fluorophore concentration variation based on the derivation of the diffusion equation. Journal of the Optical Society of America A: Optics and Image Science, and Vision, 2015, 32, 1993.	1.5	8
158	Image reconstruction for synchronous data acquisition in fluorescence molecular tomography. Journal of X-Ray Science and Technology, 2015, 23, 463-472.	1.0	0
159	Compressed sensing for high frame rate, high resolution and high contrast ultrasound imaging. , 2015, 2015, 1552-5.		8
160	Compressed sensing for synthetic transmit aperture. , 2015, , .		0
161	High line-density pulse wave imaging for local pulse wave velocity estimation using motion matching: A feasibility study on vessel phantoms. , 2015, , .		0
162	Robotized High Intensity Focused Ultrasound (HIFU) system for treatment of mobile organs using motion tracking by ultrasound imaging: An in vitro study. , 2015, 2015, 2571-5.		10

#	Article	IF	CITATIONS
163	Pulse wave velocity measurement in healthy and diseased carotid arteries in vivo. , 2015, , .		Ο
164	Nanohybrid Liposomal Cerasomes with Good Physiological Stability and Rapid Temperature Responsiveness for High Intensity Focused Ultrasound Triggered Local Chemotherapy of Cancer. ACS Nano, 2015, 9, 1280-1293.	14.6	130
165	Full-direct method for imaging pharmacokinetic parameters in dynamic fluorescence molecular tomography. Applied Physics Letters, 2015, 106, .	3.3	21
166	Bayesian Framework Based Direct Reconstruction of Fluorescence Parametric Images. IEEE Transactions on Medical Imaging, 2015, 34, 1378-1391.	8.9	29
167	Reconstruction of Fluorophore Concentration Variation in Dynamic Fluorescence Molecular Tomography. IEEE Transactions on Biomedical Engineering, 2015, 62, 138-144.	4.2	12
168	A Flexible Ultrasound Transducer Array with Micro-Machined Bulk PZT. Sensors, 2015, 15, 2538-2547.	3.8	50
169	Acceleration of dynamic fluorescence molecular tomography with principal component analysis. Biomedical Optics Express, 2015, 6, 2036.	2.9	8
170	Fluorescence molecular tomography reconstruction via discrete cosine transform-based regularization. Journal of Biomedical Optics, 2015, 20, 055004.	2.6	25
171	Direct reconstruction method for time-domain fluorescence molecular lifetime tomography. Optics Letters, 2015, 40, 4038.	3.3	8
172	Performance comparison of rigid and affine models for motion estimation using ultrasound radio-frequency signals. IEEE Transactions on Ultrasonics, Ferroelectrics, and Frequency Control, 2015, 62, 1928-1943.	3.0	24
173	Fast reconstruction in fluorescence molecular tomography using data compression of intra- and inter-projections. Chinese Optics Letters, 2015, 13, 071002-71006.	2.9	4
174	In vivo tomographic imaging with fluorescence and MRI using tumor-targeted dual-labeled nanoparticles. International Journal of Nanomedicine, 2014, 9, 33.	6.7	50
175	Safety of fast cardiac imaging using multiple transmit beams: Experimental verification. , 2014, , .		5
176	A feasibility study of carotid elastography for risk assessment of atherosclerotic plaques validated by magnetic resonance imaging. Proceedings of SPIE, 2014, , .	0.8	1
177	Depth compensation in fluorescence molecular tomography using an adaptive support driven reweighted L1-minimization algorithm. Proceedings of SPIE, 2014, , .	0.8	3
178	A dual-excitation approach for dynamic fluorescence molecular tomography. , 2014, , .		0
179	Projected restarted framework for tomographic reconstruction. Proceedings of SPIE, 2014, , .	0.8	0
180	Subsurface fluorescence molecular tomography with prior information. Applied Optics, 2014, 53, 402.	1.8	4

#	Article	IF	CITATIONS
181	An adaptive support driven reweighted L1-regularization algorithm for fluorescence molecular tomography. Biomedical Optics Express, 2014, 5, 4039.	2.9	21
182	A new ultrasound imaging indicator for vulnerability evaluatation of carotid atherosclerotic plaques. , 2014, , .		0
183	Wide-angle tissue Doppler imaging at high frame rate using multi-line transmit beamforming: An in-vivo pilot study. , 2014, , .		1
184	Resolving fluorophores by unmixing multispectral fluorescence tomography with independent component analysis. Physics in Medicine and Biology, 2014, 59, 5025-5042.	3.0	15
185	Effects of key parameters on the performance of local pulse wave velocity measurement: Theroretial analysis and in-vivo validation. , 2014, , .		1
186	Effects of key parameters on the accuracy and precision of local pulse wave velocity measurement by ultrasound imaging. , 2014, 2014, 2877-80.		2
187	Enhanced spatial resolution in fluorescence molecular tomography using restarted L1-regularized nonlinear conjugate gradient algorithm. Journal of Biomedical Optics, 2014, 19, 046018.	2.6	39
188	A regularization-free elasticity reconstruction method for ultrasound elastography with freehand scan. BioMedical Engineering OnLine, 2014, 13, 132.	2.7	18
189	Modified forward model for eliminating the time-varying impact in fluorescence molecular tomography. Journal of Biomedical Optics, 2014, 19, 056012.	2.6	8
190	Effects of parameters on the accuracy and precision of ultrasound-based local pulse wave velocity measurement: a simulation study. IEEE Transactions on Ultrasonics, Ferroelectrics, and Frequency Control, 2014, 61, 2001-2018.	3.0	21
191	A two-step optical flow method for strain estimation in elastography: Simulation and phantom study. Ultrasonics, 2014, 54, 990-996.	3.9	40
192	A Direct Method With Structural Priors for Imaging Pharmacokinetic Parameters in Dynamic Fluorescence Molecular Tomography. IEEE Transactions on Biomedical Engineering, 2014, 61, 986-990.	4.2	32
193	Fast reconstruction of fluorescence molecular tomography via a permissible region extraction strategy. Journal of the Optical Society of America A: Optics and Image Science, and Vision, 2014, 31, 1886.	1.5	13
194	Ultrasound signal wavelet analysis to quantify the microstructures of normal and frozen tissues in vitro. Cryobiology, 2014, 68, 29-34.	0.7	4
195	<i>In vivo</i> tomographic imaging of lung colonization of tumour in mouse with simultaneous fluorescence and Xâ€ray CT. Journal of Biophotonics, 2014, 7, 110-116.	2.3	7
196	Monitoring of tumor response to cisplatin with simultaneous fluorescence and positron emission tomography: a feasibility study. Journal of Biophotonics, 2014, 7, 889-896.	2.3	2
197	An adaptive Tikhonov regularization method for fluorescence molecular tomography. Medical and Biological Engineering and Computing, 2013, 51, 849-858.	2.8	34
198	A hybrid reconstruction algorithm for fluorescence tomography using Kirchhoff approximation and finite element method. Medical and Biological Engineering and Computing, 2013, 51, 7-17.	2.8	8

#	Article	IF	CITATIONS
199	MAP estimation with structural priors for fluorescence molecular tomography. Physics in Medicine and Biology, 2013, 58, 351-372.	3.0	35
200	Monitoring of Tumor Response to Au Nanorod-Indocyanine Green Conjugates Mediated Therapy With Fluorescence Imaging and Positron Emission Tomography. IEEE Transactions on Multimedia, 2013, 15, 1025-1030.	7.2	6
201	360° Fourier Transform Profilometry in Surface Reconstruction for Fluorescence Molecular Tomography. IEEE Journal of Biomedical and Health Informatics, 2013, 17, 681-689.	6.3	10
202	A regularization-free Young's modulus reconstruction algorithm for ultrasound elasticity imaging. , 2013, 2013, 1132-5.		1
203	Pulse wave imaging in normal, hypertensive and aneurysmal human aortas <i>in vivo</i> : a feasibility study. Physics in Medicine and Biology, 2013, 58, 4549-4562.	3.0	60
204	A fast surface reconstruction method for fluorescence molecular tomography based on cross-beam edge back projection. Measurement: Journal of the International Measurement Confederation, 2013, 46, 1565-1571.	5.0	3
205	The effect of controlled expression of VEGF by transduced myoblasts in a cardiac patch on vascularization in a mouse model of myocardial infarction. Biomaterials, 2013, 34, 393-401.	11.4	71
206	Accelerated image reconstruction in fluorescence molecular tomography using dimension reduction. Biomedical Optics Express, 2013, 4, 1.	2.9	27
207	Separating structures of different fluorophore concentrations by principal component analysis on multispectral excitation-resolved fluorescence tomography images. Biomedical Optics Express, 2013, 4, 1829.	2.9	16
208	Efficient L1 regularization-based reconstruction for fluorescent molecular tomography using restarted nonlinear conjugate gradient. Optics Letters, 2013, 38, 3696.	3.3	39
209	Imaging of pharmacokinetic rates of indocyanine green in mouse liver with a hybrid fluorescence molecular tomography/x-ray computed tomography system. Journal of Biomedical Optics, 2013, 18, 040505.	2.6	42
210	Fluorescence Tomography Reconstruction With Simultaneous Positron Emission Tomography Priors. IEEE Transactions on Multimedia, 2013, 15, 1031-1038.	7.2	9
211	A feasibility study of ultrasound B-mode and strain imaging for risk assessment of carotid atherosclerotic plaques validated by magnetic resonance imaging. , 2013, , .		1
212	Greedy reconstruction algorithm for fluorescence molecular tomography by means of truncated singular value decomposition conversion. Journal of the Optical Society of America A: Optics and Image Science, and Vision, 2013, 30, 437.	1.5	14
213	Fast photon-boundary intersection computation for Monte Carlo simulation of photon migration. Optical Engineering, 2013, 52, 019001.	1.0	0
214	Acceleration of Early-Photon Fluorescence Molecular Tomography with Graphics Processing Units. Computational and Mathematical Methods in Medicine, 2013, 2013, 1-9.	1.3	7
215	4-D Reconstruction for Dynamic Fluorescence Diffuse Optical Tomography. IEEE Transactions on Medical Imaging, 2012, 31, 2120-2132.	8.9	23
216	Single-heartbeat electromechanical wave imaging with optimal strain estimation using temporally unequispaced acquisition sequences. Physics in Medicine and Biology, 2012, 57, 1095-1112.	3.0	28

#	Article	IF	CITATIONS
217	Tomographic imaging of ratiometric fluorescence resonance energy transfer in scattering media. Applied Optics, 2012, 51, 5044.	1.8	Ο
218	Weighted depth compensation algorithm for fluorescence molecular tomography reconstruction. Applied Optics, 2012, 51, 8883.	1.8	7
219	Principal component analysis of dynamic fluorescence tomography in measurement space. Physics in Medicine and Biology, 2012, 57, 2727-2742.	3.0	8
220	Monitoring of tumor response to cisplatin by subsurface fluorescence molecular tomography. Journal of Biomedical Optics, 2012, 17, 040504.	2.6	14
221	INFLUENCE OF LIMITED-PROJECTION ON FLUORESCENCE MOLECULAR TOMOGRAPHY. Journal of Innovative Optical Health Sciences, 2012, 05, 1250020.	1.0	4
222	Pulse wave imaging of the human carotid artery: an in vivo feasibility study. IEEE Transactions on Ultrasonics, Ferroelectrics, and Frequency Control, 2012, 59, 174-181.	3.0	121
223	Fundamental analysis and ex vivo validation of thermal lesion mapping using harmonic motion imaging for focused ultrasound (HMIFU). , 2012, , .		0
224	Biomimetic perfusion and electrical stimulation applied in concert improved the assembly of engineered cardiac tissue. Journal of Tissue Engineering and Regenerative Medicine, 2012, 6, e12-e23.	2.7	114
225	Arterial stiffness identification of the human carotid artery using the stress–strain relationship in vivo. Ultrasonics, 2012, 52, 402-411.	3.9	172
226	Reconstruction of Fluorescence Molecular Tomography Using a Neighborhood Regularization. IEEE Transactions on Biomedical Engineering, 2012, 59, 1799-1803.	4.2	9
227	Physiologic Cardiovascular Strain and Intrinsic Wave Imaging. Annual Review of Biomedical Engineering, 2011, 13, 477-505.	12.3	38
228	In-vivo pulse wave imaging for arterial stiffness measurement under normal and pathological conditions. , 2011, 2011, 567-70.		8
229	Performance Assessment of HIFU Lesion Detection by Harmonic Motion Imaging for Focused Ultrasound (HMIFU): A 3-D Finite-Element-Based Framework with Experimental Validation. Ultrasound in Medicine and Biology, 2011, 37, 2013-2027.	1.5	39
230	Aortic pulse wave velocity measured by pulse wave imaging (PWI): A comparison with applanation tonometry. Artery Research, 2011, 5, 65.	0.6	29
231	Imaging of Wall Motion Coupled With Blood Flow Velocity in the Heart and Vessels in Vivo: A Feasibility Study. Ultrasound in Medicine and Biology, 2011, 37, 980-995.	1.5	95
232	Simultaneous fluorescence and positron emission tomography for <italic>in vivo</italic> imaging of small animals. Journal of Biomedical Optics, 2011, 16, 120511.	2.6	8
233	A comprehensive framework for Harmonic Motion Imaging for Focused Ultrasound (HMIFU) with ex vivo validation. , 2011, , .		1
234	Pulse Wave Ultrasound Manometry (PWUM): Measuring central blood pressure non-invasively. , 2011, ,		2

#	Article	IF	CITATIONS
235	Pulse Wave Imaging (PWI) and arterial stiffness measurement of the human carotid artery: An in vivo feasibility study. , 2011, , .		2
236	Non-invasive measurement of local pulse pressure by pulse wave-based ultrasound manometry (PWUM). Physiological Measurement, 2011, 32, 1653-1662.	2.1	33
237	Simultaneous imaging of wall motion and flow velocity in the hearts and vessels of mice in vivo: A feasibility study. , 2011, , .		Ο
238	Noninvasive electromechanical wave imaging and conduction-relevant velocity estimation in vivo. Ultrasonics, 2010, 50, 208-215.	3.9	44
239	In vivo characterization of the aortic wall stress–strain relationship. Ultrasonics, 2010, 50, 654-665.	3.9	50
240	Simulation Study of Amplitude-Modulated (AM) Harmonic Motion Imaging (HMI) for Stiffness Contrast Quantification with Experimental Validation. Ultrasonic Imaging, 2010, 32, 154-176.	2.6	22
241	A fast motion and strain estimation method. , 2010, , .		3
242	Response to "Potentials and Pitfalls of Local PWV Measurements". American Journal of Hypertension, 2010, 23, 935-935.	2.0	2
243	A fast normalized cross-correlation calculation method for motion estimation. IEEE Transactions on Ultrasonics, Ferroelectrics, and Frequency Control, 2010, 57, 1347-1357.	3.0	303
244	Pulse Wave Imaging for Noninvasive and Quantitative Measurement of Arterial Stiffness In Vivo. American Journal of Hypertension, 2010, 23, 393-398.	2.0	137
245	Simulation of HMIFU (Harmonic Motion Imaging for Focused Ultrasound) with in-vitro validation. , 2010, , .		3
246	Regional measurement of arterial stiffness using Pulse Wave Imaging (PWI): Phantom validation and preliminary clinical results. , 2010, , .		2
247	Characterization of the stress-strain relationship of the abdominal aortic wall in vivo. , 2009, 2009, 1960-3.		4
248	Key parameters for precise lateral displacement estimation in ultrasound elastography. , 2009, 2009, 4407-10.		2
249	Pulse Wave Imaging of Normal and Aneurysmal Abdominal Aortas <i>In Vivo</i> . IEEE Transactions on Medical Imaging, 2009, 28, 477-486.	8.9	95
250	Effects of Various Parameters on Lateral Displacement Estimation in Ultrasound Elastography. Ultrasound in Medicine and Biology, 2009, 35, 1352-1366.	1.5	64
251	Fundamental analysis of lateral displacement estimation quality in ultrasound elastography. , 2009, , .		4
252	Fundamental performance assessment of 2-D myocardial elastography in a phased-array configuration.	3.0	26

#	Article	IF	CITATIONS
253	A composite high-frame-rate system for clinical cardiovascular imaging. IEEE Transactions on Ultrasonics, Ferroelectrics, and Frequency Control, 2008, 55, 2221-2233.	3.0	93
254	Fundamental performance assessment of 2-D myocardial elastography in a phased array configuration. , 2008, , .		3
255	High-frame rate, full-view myocardial elastography with automated contour tracking in murine left ventricles in vivo. IEEE Transactions on Ultrasonics, Ferroelectrics, and Frequency Control, 2008, 55, 240-248.	3.0	72
256	Pulse wave imaging of human abdominal aortas in vivo. , 2008, , .		0
257	11B-5 Pulse Wave Imaging Of Abdominal Aortic Aneurysms: Comparison Between Control And Angiotensin II-Treated Mice In Vivo. Proceedings IEEE Ultrasonics Symposium, 2007, , .	0.0	Ο
258	AUTOMATED CONTOUR TRACKING FOR MYOCARDIAL ELASTOGRAPHY IN VIVO. , 2007, , .		2
259	10B-6 A Composite Imaging Technique for High Frame-Rate and Full-View Cardiovascular Ultrasound and Elasticity Imaging. Proceedings IEEE Ultrasonics Symposium, 2007, , .	0.0	7
260	9C-5 2D Simulation of the Harmonic Motion Imaging (HMI) with Experimental Validation. Proceedings IEEE Ultrasonics Symposium, 2007, , .	0.0	1
261	P4A-1 Automated Contour Tracking For High Frame-Rate, Full-View Myocardial Elastography In Vivo. Proceedings IEEE Ultrasonics Symposium, 2007, , .	0.0	Ο
262	9A-1 Experimental Assessment of Angle-Independent Myocardial Elastography Performance Using a Left-Ventricular Phantom Undergoing Physiologic Motion. Proceedings IEEE Ultrasonics Symposium, 2007, , .	0.0	1
263	P4A-2 An In-Vivo Study of Frame Rate Optimization for Myocardial Elastography. Proceedings IEEE Ultrasonics Symposium, 2007, , .	0.0	6
264	A Novel Noninvasive Technique for Pulse-Wave Imaging and Characterization of Clinically-Significant Vascular Mechanical Properties <i>In Vivo</i> . Ultrasonic Imaging, 2007, 29, 137-154.	2.6	99
265	11B-1 Noninvasive Electromechanical Wave Imaging and Conduction Velocity Estimation In Vivo. Proceedings IEEE Ultrasonics Symposium, 2007, , .	0.0	5
266	Mapping of Regional Cancerous Tissue Mechanical Property Changes Using Harmonic Motion Imaging. , 2007, , .		1
267	Myocardial Elastography at Both High Temporal and Spatial Resolution for the Detection of Infarcts. Ultrasound in Medicine and Biology, 2007, 33, 1206-1223.	1.5	84
268	AneuMastat reduces aneurysm incidence in the angiotensin II (AngII)-induced model of abdominal aortic aneurysm (AAA) in the wildtype C57BL6 mouse. Journal of the American College of Surgeons, 2007, 205, S111.	0.5	1
269	Imaging the mechanics and electromechanics of the heart. , 2006, Suppl, 6648-51.		15
270	Application of the wavelet transforms on axial strain calculation in ultrasound elastography. Progress in Natural Science: Materials International, 2006, 16, 942-947.	4.4	41

JIANWEN LUO

#	Article	IF	CITATIONS
271	Elasticity reconstruction for ultrasound elastography using a radial compression: An inverse approach. Ultrasonics, 2006, 44, e195-e198.	3.9	13
272	Detection of murine infarcts using myocardial elastography at both high temporal and spatial resolution. , 2006, 2006, 1552-5.		4
273	2I-4 Pulse Wave Imaging in Murine Abdominal Aortas: A Feasibility Study. , 2006, , .		1
274	Detection of murine infarcts using myocardial elastography at both high temporal and spatial resolution. Annual International Conference of the IEEE Engineering in Medicine and Biology Society, 2006, , .	0.5	0
275	Savitzky–Golay smoothing and differentiation filter for even number data. Signal Processing, 2005, 85, 1429-1434.	3.7	264
276	Properties of Savitzky–Golay digital differentiators. , 2005, 15, 122-136.		248
277	Axial strain calculation using a low-pass digital differentiator in ultrasound elastography. IEEE Transactions on Ultrasonics, Ferroelectrics, and Frequency Control, 2004, 51, 1119-1127.	3.0	110
278	Theoretical analysis of tissue axial stretching model in elastography*. Progress in Natural Science: Materials International, 2004, 14, 430-438.	4.4	0
279	Estimation and reduction of decorrelation effect due to tissue lateral displacement in elastography. IEEE Transactions on Ultrasonics, Ferroelectrics, and Frequency Control, 2002, 49, 541-549.	3.0	8